A simplified methodology to identify material parameters of a hyperelasto-visco-hysteresis model: application to a fluoro-elastomer

Hervé Laurent, Aude Vandenbroucke, Gérard Rio, Nourredine Aït Hocine

A simplified methodology to identify material parameters of a Hyperelasto-Visco-Hysteresis model: application to a fluoro-elastomer

H. Laurent[1], A. Vandenbroucke[1], G. Rio[1], N. Aït Hocine[2]

[1] Université Européenne de Bretagne,
Université de Bretagne-Sud,
Laboratoire d'Ingénierie des MATériaux de Bretagne,
(LIMATB / Equipe Génie Mécanique et Matériaux),
BP 92116, 56321 Lorient cedex, France.
[2] Laboratoire de Mécanique et Rhéologie (LMR)
Ecole Nationale d'Ingénieurs du Val de Loire,
Rue de la chocolaterie, BP 3410, 41034, Blois cedex France.

E-mail: herve.laurent@univ-ubs.fr

Abstract.

This paper presents a method to identify material parameters of a Hyperelasto-Visco-Hysteresis (HVH) model and its application for the simulation of a fluoro-elastomer behaviour. This 3D-phenomenological model is based on the additive decomposition of three stress components. Each of these constitutive stresses is related to a physical phenomenon that occurs during mechanical loading: a hyperelastic equilibrium stress response, an irreversible pure hysteresis stress contribution and a rate-dependent viscoelastic stress behaviour.

In order to independently identify these parts of the model, an experimental campaign, including multi-step relaxation in traction and compression tests and simple relaxation in tension and compression tests, is used. The hysteretic and hyperelastic contributions are identified considering only the state at the end of the relaxation periods of the multi-step relaxation tests. The viscoelastic response is analytically calculated with the simple relaxation test. As an advantage, the developed identification scheme gives the possibility to discriminate all the stress components of the model. Finally, the numerical simulation of a seal in relaxation is carried out to verify the capability of the proposed HVH model by reproducing the mechanical response of the studied material.

PACS numbers: 83.80.Wx,83.60.La,83.85.St,02.70.Dh,46.15.-x,46.35.+z

1. Introduction

Elastomeric rubbers are substantially used in engineering applications, notably in the automotive industry for sealant materials, engine mounts, bushes and tires... Thus, the accurate prediction of their mechanical behaviour under operational conditions is paramount to the industry.

The mechanical behaviour of these materials is dominated by a nonlinear strain rate-dependent response. Futhermore, under cyclic loading, these materials also exhibit other inelastic behaviours, such as the Mullins effect [1] and hysteresis phenomena [2]. These nonlinear elastic behaviours are classically modelled using either a physical description of molecular network theories [3, 4, 5, 6] or phenomenological approaches [7, 8, 9]. The strain energy expression obtained from a molecular theory is often complex and material specific. However, some new micro-mechanical models seem promising (*i.e.* [10, 11]). With the phenomenological approach, material is treated as a continuum body and a strain energy density is postulated, usually in terms of the deformation invariants, generally strain or stretch invariants [12]. Descriptions of many of the models proposed can be found in [13, 14, 15, 16, 12, 17, 18].

In mechanical engineering, one of the main challenges for the constitutive relationships, is the development of a simple material parameter identification method. Indeed, the behaviour model, as well as the identified material parameters, must correlate well with the experimental results for any given stress state, must provide stable results for all types of loading, and must be applicable to a wide range of materials [19, 12]. However, for elastomers, several material parameters are usually required to reflect the nonlinearity in the stress-strain response, the strain-rate dependent response, etc.

In a previous study [20], several experimental tests were carried out to verify the strain-rate dependent response, the tension and compression behaviours during cyclic loading, as well as the relaxation behaviour for loading in tension and compression of a fluoro-elastomer Viton material. An original phenomenological model, called Hyperelasto-Visco-Hysteresis (HVH), has also been used to simulate this complex behaviour. This model, written in 3D and implemented in an in-house code *HEREZH++* [21], is based on the superimposition of three stress components which correspond to linear viscoelastic, hyperelastic and pure hysteresis behaviour. It takes the phenomena of viscosity, possible compressibility and hysteresis into account. The viscosity is described with two linear Maxwell elements which seem sufficient for an adequate representation of the viscoelastic behaviour. The stress tensor deviatoric part of the hysteretic contribution simulates the rate-independent irreversibility of the mechanical behaviour. Contrary to previous studies based on the same model [22, 23, 24, 25, 26, 27], hyperelastic contribution is simulated with the Hart-Smith strain energy density function, which depends only on strain invariants. The Hart-Smith hyperelastic potential is thought to provide good correlation between the experimental and simulation results [28, 29]. Furthermore, this potential is extended to take the

influence of compressibility on rubber materials into account.

In the aforementioned study, an optimisation procedure was also done to minimise the experimental data and prediction of the tests by a full numerical resolution. A least-square method implemented in the *SiDoLo* code [30, 31] and linked to *HEREZH++* was used. The applied method consists in using all experimental tests indiscriminately to identify the material parameters of each contribution. Unfortunately, the error function generally does not lead to a single optimised solution. For example, the best solution, both in tension and compression tests, involves a negligible hysteresis contribution, whereas the hyperelastic contribution is the most important. One of the main conclusions of this work is that better identification of the material parameters is necessary.

The aim of this paper is to propose a new identification method of the HVH model parameters using a fluoro elastomer. New cyclic tension and compression tests interrupted by relaxation steps (multi-step relaxation tests) are performed to characterise different behaviours, such as hyperelasticity, hysteresis and viscosity. The original identification method is carried out in two different stages with a minimal use of the numerical inverse procedure. The first stage consists in the identification of hyperelastic and hysteretic contributions. Thus, the multi-step relaxation tests are used considering only the state at the end of the relaxation periods, the *equilibrium hysteresis* state [32]. In the second stage, the viscous parameters are determined from relaxation in tension and compression tests. An analytical identification is used to obtain the two characteristic times of both Maxwell elements. The main advantage of this method is that, using only this multi-step relaxation test, hyperelasticity, hysteresis and viscosity contributions are discriminated, which results on the substantially easy and simple identification process of the material parameters.

To verify the pertinence of the obtained material parameters, experimental tests that were not used for the identification, are simulated. A good performance of the proposed model is shown by a comparative analysis between the predictive solution and experimental data. Moreover, despite the fact that material parameters are identified from only the first cycle of experimental tests, the simulation of cyclic loading tests show that some aspects of the Mullins effect can be predicted. Finally, an o-ring seal is modelled in relaxation in using the HVH model and the results are compared to experimental data and discussed.

2. Material and experimental conditions

Experimental tests including cyclic tension, cyclic compression and relaxation tests, are achieved in similar conditions that are described in [20]. These tests were carried out on a Viton (a fluoro-polymer) elastomer. This material is commonly called "FKM elastomer" according to the D1418 ASTM norm. This fluoro-elastomer is mainly used for sealing operations, over a wide range of temperatures and pressures, under a given compression in groove. Thus, such seals undergo relaxation phenomena. Therefore, in

this study, we particularly focus on the first cycle of loading in compression and tension. However, only minor adaptation of the identification procedure is required to simulate the steady state behaviour of rubber material after cyclic loading tests.

2.1. Cyclic tests interrupted by relaxation steps

Multi-step relaxation tests were carried out at room temperature with a strain rate of 3.3×10^{-3} s^{-1} corresponding to a crosshead speed of 5 mm/min. This strain rate is defined as $\dot{\varepsilon} = \dot{\Delta l}/l_0$ with $\Delta l = l - l_0$ which denotes the variation of the initial length of the specimen in compression or in tension tests. Cyclic tests are carried out up to 30% and 50% of the deformation, respectively, in compression (figure 1) and in tension (figure 2). The imposed displacement was interrupted by several hold times at constant strains of 10, 20 and 30% in compression and 10, 20, 30, 40 and 50% in tension, both during the loading and the unloading, as can be seen in figures 1 to 2. The obtained results are shown in terms of first Piola-Kirchhoff stress (PK1 stress or engineering stress) versus stretch.

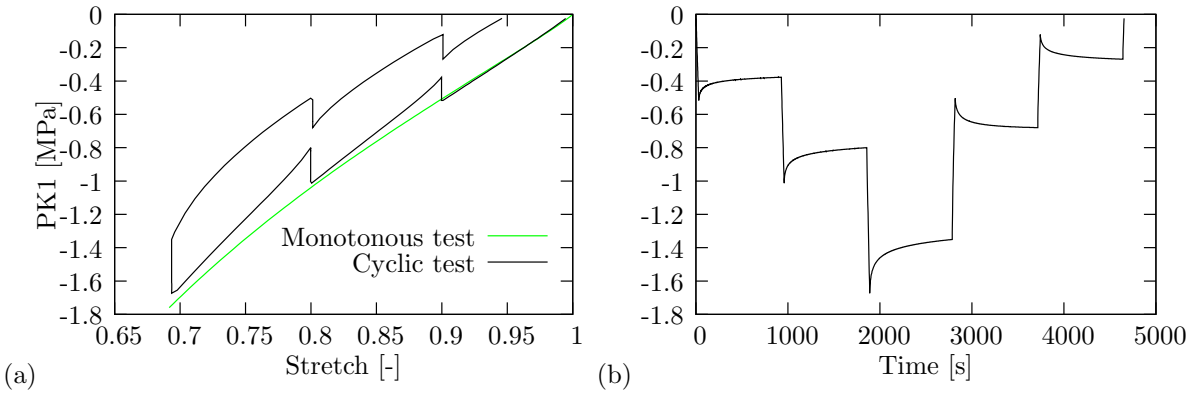

Figure 1. Cyclic compression tests interrupted by relaxation steps. (a) Stress-stretch response. (b) Stress-time response.

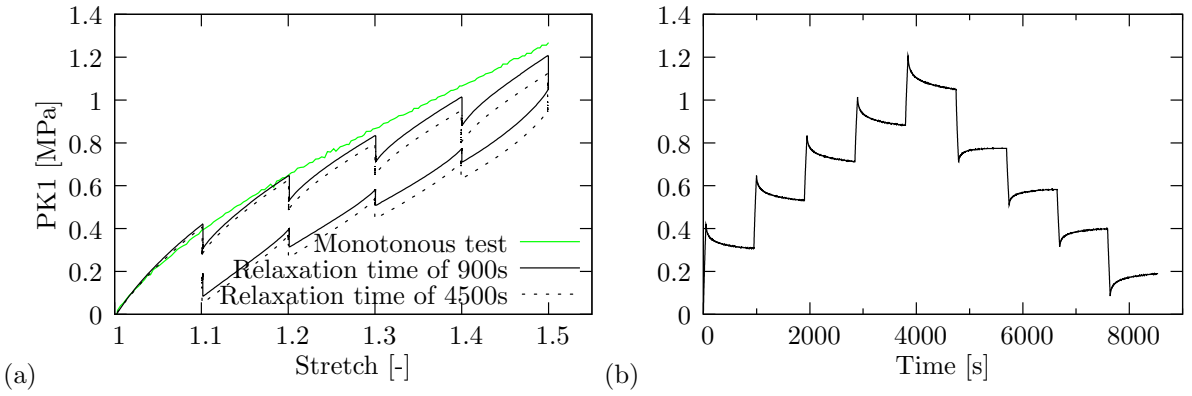

Figure 2. Cyclic tension tests interrupted by relaxation steps. (a) Stress-stretch response. (b) Stress-time response.

These figures clearly show that the stress decreases during the relaxation segments in loading, and that the stress increases during the relaxation segments in unloading (which correlates well with results that can be found in the literature [26, 33, 34, 35, 36, 37, 38]). At the end of these relaxation periods, termination points of the hold times correspond to time equilibrium states, called *equilibrium hysteresis* by Lion [34]. According to several authors, this behaviour may be attributed to an irreversible slip process between fillers in the rubber microstructures [39, 40], which is the resulting phenomenon of rubber-filler bonds breaking [37, 41, 42]. The difference between the equilibrium stress and the total stress is the overstress of the viscous part of the stress.

Figure 2(a) shows stress-stretch curves of cyclic tension interrupted by relaxation times during 900s and 4500s. Except for large stretch, due to the reduction of the maximun stress after each relaxation step, the same equilibrium state appears in both cases. For the 900s relaxation time, the hysteresis area is 0.45 MPa, while it is 0.41 MPa for the 4500s relaxation time which leads to a difference of 8% between these two conditions. We, therefore, consider that a 900s relaxation time is sufficiently long to reach the equilibrium state and to obtain the non-viscous hysteresis part of the material behaviour.

Figures 1(a) and 2(a) also show the corresponding compression and tension monotonous behaviours, respectively. The multiple step stress relaxation curves follow the monotonous tests. As can be seen, the mechanical behaviour of the Viton is not modified by relaxation processes at this strain rate. This suggests that relaxation processes do not alter the internal structure of the studied elastomer during loading. Such results correlate with those found in the literature on the polymer Adiprene-L100 [43].

2.2. Influence of the strain rate on compression tests

Figure 3 shows the same previous tests (with a relaxation time of 900 s), but with different values of the strain rate. Similar termination points of the hold times are observed for all strain rates, which means that the equilibrium states do not seem to be influenced by the strain rate.

3. Hyperelasto-Visco-Hysteresis model

3.1. General motivation

From a macroscopical point of view, the mechanical response of Viton, presented in Section 2, exhibits three main phases, namely a reversible elastic phase which occurs at the onset of the loading, a strain rate dependent phase which can be described in terms of the viscosity, and an irreversible plastic phase (hysteresis response) which occurs during the loading-unloading cycles. The Hyperelasto-Visco-Hysteresis model discerns these physical phenomena and superimposes them so as to reasonably predict the global macroscopic behaviour of the studied material. This approach assumes a

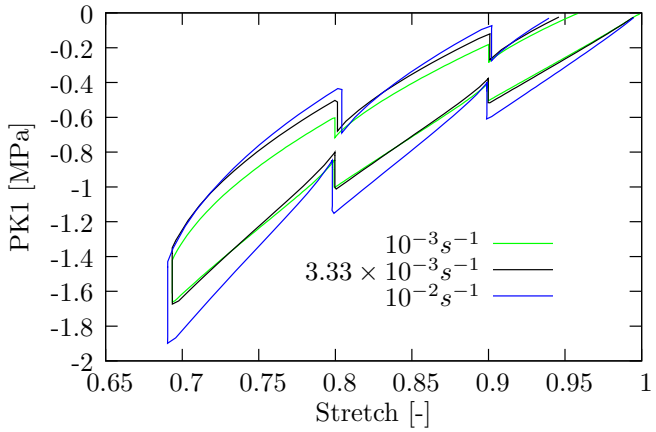

Figure 3. Cyclic compression stress-stretch curves for several strain rates.

superimposition of stress contributions instead of strain ones. Such an assumption has already been adopted by several authors for rubbers and polymeric materials [38, 44, 45, 46, 47].

According to the HVH rheological diagram presented in figure 4, a given applied stress is the sum of several stress components, each one is related to a physical phenomenon that occurs during mechanical loading. The global applied stress to the material is, therefore, the sum of the hyperelastic $\boldsymbol{\sigma_e}$, viscoelastic $\boldsymbol{\sigma_v}$ and pure hysteretic $\boldsymbol{\sigma_h}$ stress components as follows:

$$\boldsymbol{\sigma} = \boldsymbol{\sigma_e} + \boldsymbol{\sigma_v} + \boldsymbol{\sigma_h} \tag{1}$$

where $\boldsymbol{\sigma_e}$, $\boldsymbol{\sigma_v}$ and $\boldsymbol{\sigma_h}$ are defined by a specific constitutive equation.

Some classical viscoelastic models reasonably reproduce hysteresis phenomena, but the HVH model distinguishes the viscoelastic and the non-viscous hysteretic behaviour. The pure hysteresis component $\boldsymbol{\sigma_h}$ models the rate-independent irreversibilities of the mechanical behaviour. It is a function of the current strain $\boldsymbol{\varepsilon}$ and of its history between a reference and the current states. The viscoelastic stress component $\boldsymbol{\sigma_v}$ is a function of the strain rate $\dot{\boldsymbol{\varepsilon}}$ and its integration. A generalised Maxwell model is used to simulate this stress contribution. The nonlinear elasticity $\boldsymbol{\sigma_e}$ is represented by a hyperelastic constitutive equation depending on the strain invariants.

Figure 4 illustrates the HVH rheological model in a one-dimensional schema, in which each stress component is presented by a set of rheological branches. The HVH mechanical behaviour is also qualitatively illustrated in figure 5 with the proportion of each component $\boldsymbol{\sigma_e}$, $\boldsymbol{\sigma_v}$ and $\boldsymbol{\sigma_h}$ and with total stress $\boldsymbol{\sigma}$. This figure shows that the result of the stress superimposition presents the typical shape of this fluoro-elastomer stress-strain cycles with relaxation periods. Figure 5(c) exhibits the effect of the hysteretic stress component $\boldsymbol{\sigma_h}$, which makes points b, d, h and j different at the end of ab, cd, gh and ij relaxation periods. In the case of viscoelastic behaviour, these ends of relaxation periods are coincident (figure 5(b)).

To implement this constitutive law in a numerical schema, a 3D finite deformation

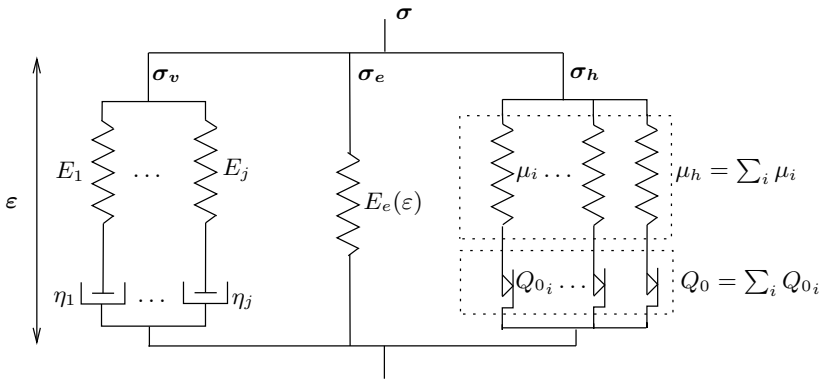

Figure 4. HVH model in one-dimensional case with viscous, hyperelastic and hysteresis contributions.

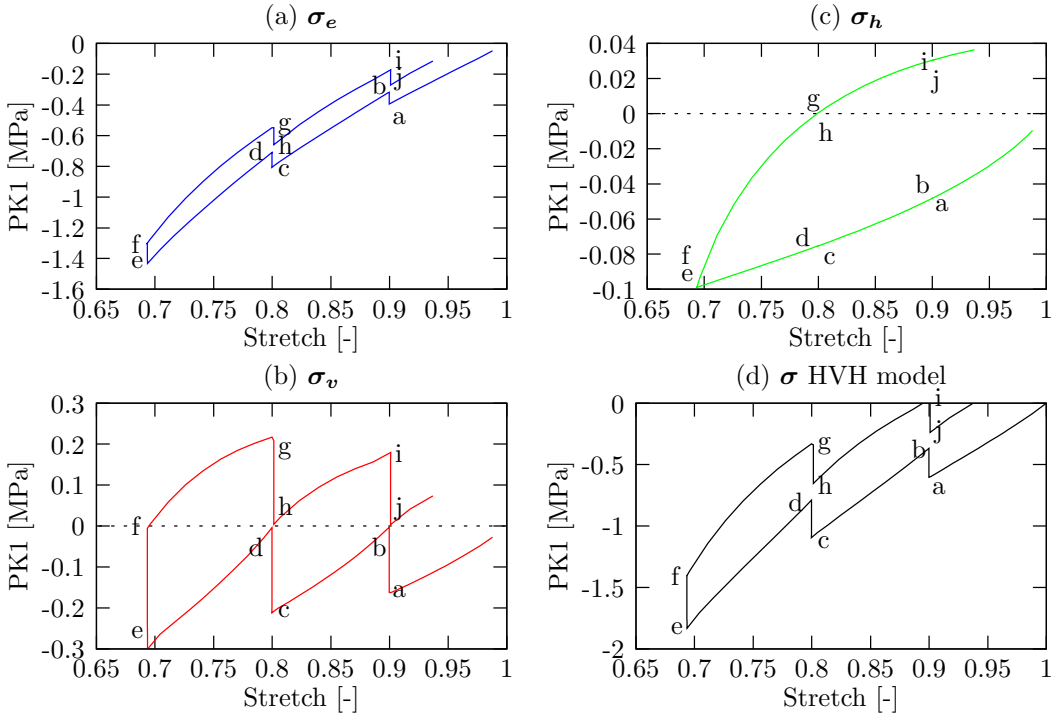

Figure 5. Cyclic behaviour of the three stress components of the HVH model in the cyclic compression test interrupted by relaxation steps on the fluoro-elastomer.

framework has been developed in a finite element software, called HEREZH++ [21]. An Eulerian formulation, the Cauchy stress tensor $\boldsymbol{\sigma}$, the Almansi strain tensor $\boldsymbol{\varepsilon}$ and the Jaumann time derivative of the stress are chosen for this purpose [48, 49]. The consistent of this model with the second law of thermodynamic has been verified by G. Blès [50].

3.2. Hysteresis

For the hysteresis response, rheological models containing elastic and slip elements are considered as derived from a general pure hysteresis model [51]. It represents the non-viscous hysteresis part of the mechanical behaviour during cyclic tests.

It is important to notice that the hysteresis contribution is taken into account according to an incremental evolution like an elasto-plastic classical formulation. The originality of this evolution is to have a dependancy of several reference states named discrete memory states (like inversion and crossing states) which are representative of the loading history. These several states are managed by an inversion point algorithm. These explanations of state management in the case of the simulation of the uniaxial tensile test can be found in [52, 53]. The hysteresis model is then adapted to the simulation of the cyclic loading condition.

We assume that the material is isotropic and that the hysteresis contribution is only deviatoric. Thus, the deviatoric part of the Cauchy stress tensor corresponds to the hysteresis contribution $\boldsymbol{S_h}$. This stress deviatoric tensor is obtained through time integration (Jaumann time derivative) of the following incremental constitutive relation:

$$\dot{\boldsymbol{S_h}} = 2\,\mu_h\,\bar{\boldsymbol{D}} + \beta\;.\;\phi\left(\Delta_r^t\boldsymbol{S_h}, \bar{\boldsymbol{D}}\right)\;.\;\Delta_r^t\boldsymbol{S_h} \tag{2}$$

In this relation:

- μ_h represents the shear Lamé coefficient;
- $\bar{\boldsymbol{D}}$ denotes the deviatoric strain rate tensor;
- $\Delta_r^t\boldsymbol{S_h}$ describes the evolution of the deviatoric part of the hysteretic stress tensor between a reference state r and current state t. At the beginning of the loading, the reference state is the initial state, *i.e.* $r = 0$. For other paths, the reference point is the previous inversion state as long as no crossing point has been detected (more information on the management of these reference states can be found in [26, 52, 53]);
- $\beta = \dfrac{-2\mu_h}{(\omega' Q_0)^{n_p}(Q_{\Delta\boldsymbol{s_h}})^{2-n_p}}$ where:
  $Q_{\Delta\boldsymbol{s_h}} = \sqrt{\mathrm{tr}\left(\Delta_r^t\boldsymbol{S_h} : \Delta_r^t\boldsymbol{S_h}\right)}$ is relative to the intensity of $\Delta_r^t\boldsymbol{S_h}$;
- $\phi\left(\Delta_r^t\boldsymbol{S_h}, \bar{\boldsymbol{D}}\right) = \mathrm{tr}\left(\Delta_r^t\boldsymbol{S_h}.\bar{\boldsymbol{D}}\right) - \dfrac{\left(Q_{\Delta\boldsymbol{s_h}}\right)^2}{2\mu_h}\;.\;\dfrac{\dot{\omega'}}{\omega'}$ denotes the non-reversible intrinsic dissipated rate function;
- parameter $\omega' = \omega\cos(j)$ denotes the Masing similarity function. Along the first loading path, ω' is equal to 1 and the reference state is the initial state. In the case of other paths, ω' is equal to $2\cos(j)$ where j denotes the angle between the directions of the stress tensor, expressed in the deviatoric plane (*i.e.* in the classical polar orientation of the tensor, before and after the last reference point);
- n_p is Prager's parameter, which is chosen to change the shape of the function in the transition shape. Explanations of this parameter can also be found in [26].

The parameters of the hysteretic stress component $\boldsymbol{S_h}$ are coefficient μ_h, yield hysteresis Q_0 and Prager's parameter n_p.

The inversion point and crossing point are managed with the previously defined intrinsic dissipation rate function $\phi\left(\Delta_r^t \boldsymbol{S_h}, \bar{\boldsymbol{D}}\right)$. This value is related to a volume element and must always be positive. Thus, at the reference state $\phi = 0$ and the state at time t is an inversion point when function ϕ becomes negative.

3.3. Hyperelasticity

The isotropic hyperelastic response of rubber-like materials is commonly described by the use of an arbitrary strain energy density function $\mathcal{W}$ depending only on strain invariants [54, 7, 55, 9, 17]. Several hyperelastic potentials have been tested and the Hart-Smith's model seemed to better describe the hyperelastic part of the studied material. This potential enables a good approximation of the sharp upturn at large strains because its strain-hardening response is taken into account by an exponential function [55, 29]. The deviatoric part of this model is given by the following equation:

$$\mathcal{W}_d = C_1 \int_3^{J_1} \exp\left[C_3 (J_1 - 3)^2\right] \, dJ_1 + C_2 \log\left(\frac{J_2}{3}\right) \tag{3}$$

where C_1, C_2 and C_3 are the material parameters. This potential depends on strain invariants: $J_1 = I_1 . I_3^{-1/3}$ and $J_2 = I_2 . I_3^{-2/3}$ with I_1 and I_2 written in terms of the left Cauchy-Green tensor $\boldsymbol{B}$:

$$I_1(\boldsymbol{B}) = \mathrm{tr}\,(\boldsymbol{B}) \,; I_2(\boldsymbol{B}) = \frac{1}{2}\left[\left(\mathrm{tr}\,(\boldsymbol{B})\right)^2 - \mathrm{tr}\left(\boldsymbol{B}^2\right)\right] \tag{4}$$

This model has been extended for compressible materials. To take this compressibility into account, an additive decomposition of hyperelastic potential in the deviatoric and volumetric parts is used [56]:

$$\mathcal{W} = \mathcal{W}_d(J_1, J_2) + \mathcal{W}_v(I_3) \tag{5}$$

in which the volumetric part is expressed under the form:

$$\mathcal{W}_v(I_3) = \frac{K}{2}(V - 1)^2 \tag{6}$$

where K is the bulk modulus and $J_3 = I_3 = V^2$ with V stands for the relative change of volume.

Contrary to a classical hyperelastic evolution, with the HVH model, the representation of stress component $\boldsymbol{\sigma_e}$ during a cycle of loading-unloading leads to a loop (figure 5(a)). This phenomenon is due to the assumption of the additive decomposition of stress given by Eq. (1) and that component σ_h in the loading direction describes a cycle during a loading-unloading path (figure 5(c)). So, due to the deviatoric form of the hysteresis, in the transverse direction, the $\boldsymbol{\sigma_h}$ component also describes a cycle while the global transverse stress has to remain equal to zero. That induces a cycle on the transverse component of $\boldsymbol{\sigma_e}$ and finally also along the loading direction, due to the

small compressibility of the material. It is this inelastic evolution which prevents full elastic recovery of the component $\boldsymbol{\sigma_e}$.

The main parameters of the stress component $\boldsymbol{\sigma_e}$ are bulk modulus K, and parameters C_1, C_2 and C_3.

3.4. Viscosity

The generalised Maxwell model reasonably describes the viscoelastic behaviour of elastomers, as it gradually tends to an equilibrium elastic state during a long relaxation test (*e.g.* [57, 58, 59, 60]).

The viscoelastic Maxwell model used in the HVH model is given only by its deviatoric parts. Considering one Maxwell element composed of an elastic stiffness E and a viscous dissipative coefficient η, this deviatoric part is written as:

$$\frac{\dot{\boldsymbol{S}}_{\boldsymbol{v}}}{2\mu_v} + \frac{\boldsymbol{S_v}}{\eta} = \bar{\boldsymbol{D}} \tag{7}$$

where $\mu_v = \dfrac{E}{2(1+\nu)}$ with ν is the Poisson coefficient which is only used to simulate the 3D behaviour.

As for relaxation, at a given deformation ε_0 (or stretch λ_0) from time t_0, in the one dimensional case, the generalised Maxwell model predicts that the viscous total stress $\sigma_v(t)$ will be the sum of stresses in each single Maxwell element (figures 4 and 8) and stress $\sigma_v(t)$ tends to σ_∞ when t tends to ∞ (*e.g.* [58, 61, 37]):

$$\sigma_v(t) = \sum_{j=1}^{n} \sigma_{0j} \exp\left(-\frac{(t-t_0)}{\tau_j}\right) + \sigma_\infty \quad \forall t \geq t_0 \tag{8}$$

with $\tau_j = \dfrac{\eta_j}{E_j}$ as the relaxation times. E_j and η_j are adjustable parameters corresponding to the elastic stiffness and viscous dissipitative coefficient of each j^{th} Maxwell element, respectively.

Stress σ_∞ corresponds to the hyperelastic and hysteretic stress contributions of other branches:

$$\sigma_\infty = \sigma_e + \sigma_h \tag{9}$$

This stress response obtained at the end of the relaxation can be considered as the equilibrium stress response.

4. Material parameter identification of the HVH model

The viscous $\boldsymbol{\sigma_v}$, hyperelastic $\boldsymbol{\sigma_e}$ and hysteretic stress $\boldsymbol{\sigma_h}$ contributions are represented in figures 6(a) and 6(b) for compression and tension tests at a given stretch λ_0, based on the experimental results shown in figures 1 and 2, respectively. As mentioned above, the equilibrium state σ_∞ can be obtained by connecting all the asymptotic converged stress values at the end of the relaxation periods of each corresponding strain (or stretch)

level, according to the description of this state previously described by Lion [34]. With the hypothesis that the viscous stress $\boldsymbol{\sigma_v}$ is completely saturated at the end of these hold times, σ_∞ which is composed of hysteresis stress contribution $\boldsymbol{\sigma_h}$ and hyperelastic stress contribution $\boldsymbol{\sigma_e}$ follows the red curve in these figures.

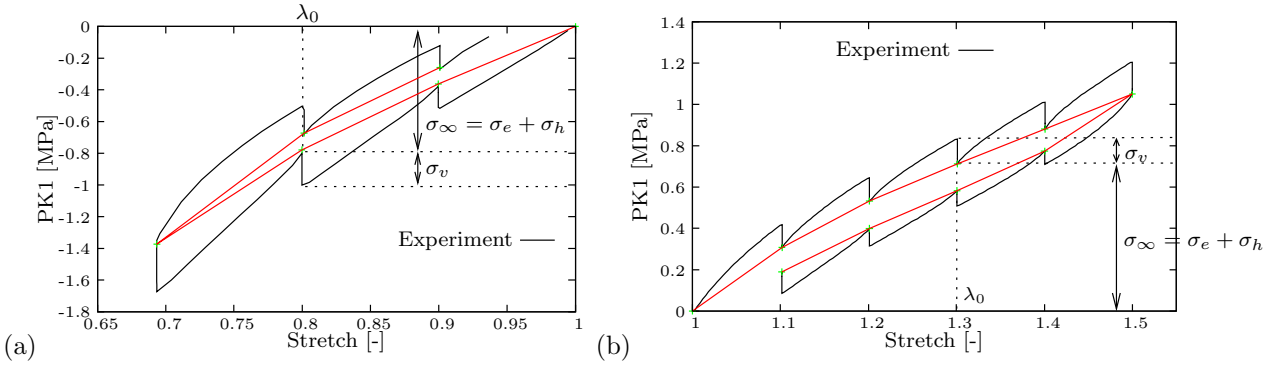

Figure 6. Estimated viscous, hyperelastic and hysteresis behaviours. (a) Compression test. (b) Tension test.

4.1. Hyperelastic and hysteresis contributions

With this assumption of stress decomposition, it is relatively easy to identify material parameters of hyperelastic $\boldsymbol{\sigma_e}$ and hysteresis $\boldsymbol{\sigma_h}$ contributions. Inverse analysis software package *SiDoLo* [30, 31] and the finite element software program *HEREZH++* [21] are used for this purpose. Experimental boundary and loading conditions are simulated with *HEREZH++* on a single hexahedral finite element to reproduce the assumed homogenous state at the center of the specimen. An interface between *SiDoLo* and *HEREZH++* allows for an optimisation of material parameters through a trial prediction-error iterative procedure [27]. Thus, only a few iterations are necessary because a starting solution is first predicted with parameters initially obtained by manual trials. This starting solution is as close as possible to the optimised solution.

The experimental database for the identification of the hyperelastic and hysteresis contributions includes the tests presented in the previous section, with only the points at the ends of the relaxation periods both in compression and tension loadings. The obtained material parameter values are reported in Table 1. The value of bulk modulus K, identified with an oedometric compression test, is equal to 2700 MPa.

Figure 7 shows the comparison between experimental equilibrium responses and model predictions. Contrary to the results reported in the previous work [20], the identified material parameters show that the hysteretic contribution is not negligible. However, the main contribution in the stress-stretch response is still controlled by the hyperelastic part.

It is also important to notice that the stress-stretch curves are not similar in tension and compression loadings. At a given stretch, stress level recorded in compression test is higher than that obtained in tension, suggesting the strong influence of compression

Hyperelastic	Hysteretic
$C_1 = 0.4$ MPa	$n_p = 0.38$
$C_2 = 0.09$ MPa	$\mu_h = 0.58$ MPa
$C_3 = 0.21$	$Q_0 = 0.09$ MPa
error = 0.0534	

Table 1. Hyperelastic and hysteretic parameters identified in tension and compression tests (K=2700 MPa).

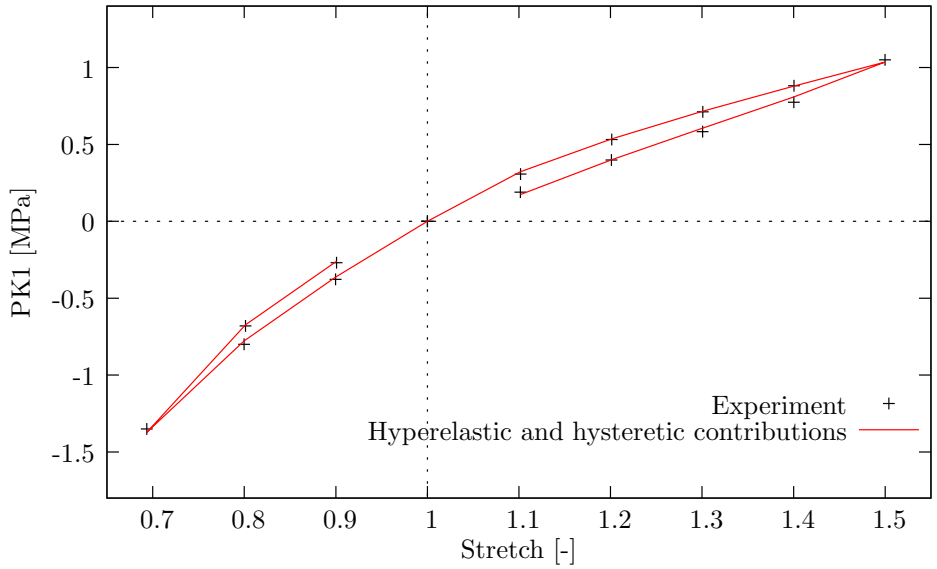

Figure 7. Comparison between experimental data and identification procedure for the hyperelastic and hysteretic contributions in tension and compression tests (only the points at the ends of the relaxation periods are presented).

loading on the material mechanical behaviour. Thus, as compression and tension data are considered together, the material parameters, presented in table 1, are a compromise of these two behaviours. Table 2 gives parameters identified from only compression experimental data. The comparison between the parameters presented in tables 1 and 2 shows only a difference in parameter C_3, which is probably related to the stiffening in stress-stretch evolution in the case of tensile test.

Hyperelastic	Hysteretic
$C_1 = 0.4$ MPa	$n_p = 0.32$
$C_2 = 0.08$ MPa	$\mu_h = 0.55$ MPa
$C_3 = 0.09$	$Q_0 = 0.1$ MPa
error = 0.0219	

Table 2. Hyperelastic and hysteretic parameters identified in compression only (K=2700 MPa).

The identification procedure is based on the minimization of an error function with a gradient type algorithm. This function is defined in the least square sense. The error function value at the end of the inverse analysis procedure is also presented in tables 1 and 2. A comparison between the error functions of two kinds of parameters shows that the fitted curves conform well to the stress-stretch data over a single mode of deformation (*e.g.* compression).

4.2. Viscosity

The viscous part is represented by the generalised Maxwell model that is shown in figure 4 and given by Eq. (7). To estimate the stiffness and viscosity parameters, E_j and η_j, combination with the number j of Maxwell elements, we apply the following procedure‡ (figure 8(a)).

First, in the one dimensional case, let us focus on a single Maxwell model:

$$\frac{d\sigma}{dt} = E_1 \left(D - \frac{\sigma}{\eta_1} \right) \tag{10}$$

with D, the strain rate. During the relaxation phase, after time $t = t_0$ in which $\sigma = \sigma_{01}$ (the stress at the end of the loading phase) and $D = 0$, the time integration of Eq. (10) gives:

$$\sigma(t) = \sigma_{01} \exp\left(-\frac{(t - t_0)}{\tau_1} \right) \quad \forall t \geq t_0 \tag{11}$$

In this case, $\forall t \geq t_0$, if we suppose that $\sigma_{01} = 1$ and $\tau_1 = \dfrac{\eta_1}{E_1} = 1$, after time t greater than $4\tau_1$, we have: $\sigma(t) = \exp(-4) \simeq 0.02$ which shows that only 2% of the first Maxwell element has an influence on the relaxation response. This suggests that we can choose between every relaxation time, a time: $t_j \geq 4\tau_j$ to describe the relaxation tests in tension and compression. Figure 8(b) gives a schematic representation of this assumption during a relaxation response. In this figure, a displacement in both time and stress has been taken into account and only the viscous part σ_v is considered.

During the loading phase (between time $t = 0$ and t_0), the time integration of Eq. (10) gives:

$$\sigma(t) = E_1 \tau_1 \, D \left(1 - \exp\left(-\frac{t}{\tau_1} \right) \right) \quad \forall \; 0 \leq t \leq t_0 \tag{12}$$

According to Eq. (8), for n Maxwell elements, this expression can be extended by:

$$\sigma(t) = D \left(\sum_{j=1}^{n} E_j \tau_j \left(1 - \exp\left(-\frac{t}{\tau_j} \right) \right) \right) \tag{13}$$

Giving the stiffness and the viscosity of each j^{th} Maxwell element:

$$E_j = \frac{\sigma_j(t_0)}{D \, \tau_j \left(1 - \exp\left(-\dfrac{t_0}{\tau_j} \right) \right)} \quad \text{and } \eta_j = \tau_j . E_j \tag{14}$$

‡ In the following procedure, σ represents the viscous part $\boldsymbol{\sigma_v}$

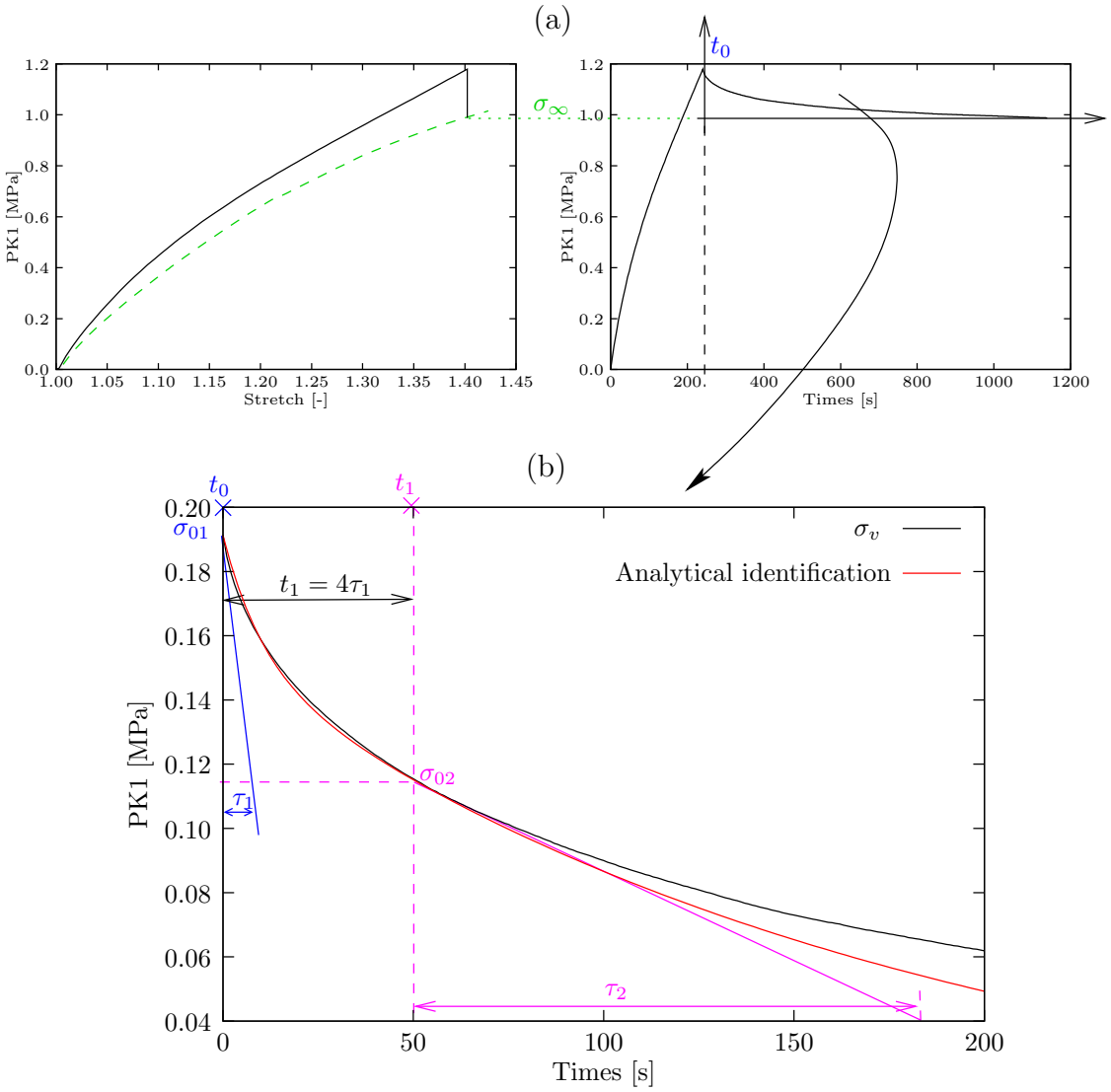

Figure 8. (a) The stress-stretch and stress-time relaxation test in tension. (b) Determination of the characteristic relaxation times τ_j in the displaced stress-time curve.

The values of $\sigma_j(t_0)$ correspond to the stress of each Maxwell element during the loading phase. They can be determined graphically from relaxation tests in compression and tension.

For example, in figure 8(b), two Maxwell elements have been used in a relaxation test in tension. With assumption $t_1 \geq 4\tau_1$, the relaxation times give:

- first Maxwell element: $t_0 = 0$s, $\tau_1 = 10.25s$ and $\sigma_{01} = 0.114$ MPa;
- second Maxwell element: $t_1 = 50$s, $\tau_2 = 176.92s$ and $\sigma_{02} = 0.191$ MPa.

According to Eq. (8), assuming that only the second Maxwell element takes place

for time $t \geq t_1$, we have:

$$\sigma(t) = \sigma_{02} \exp\left(-\frac{(t-t_1)}{\tau_2}\right) \tag{15}$$

In this case, during the loading phase:

$$\begin{aligned} \sigma_2(t_0) &= \sigma_{02} \exp\left(\frac{t_1}{\tau_2}\right) &= 0.152\,\text{MPa} \\ \sigma_1(t_0) &= \sigma_{01} - \sigma_2(t_0) &= 3.9 \times 10^{-2}\,\text{MPa} \end{aligned}$$

To obtain a single set of material parameters, both valid in relaxation tests in tension and compression, an average value of relaxation time $\bar{\tau}_j$ is chosen. With these values, using $\bar{\tau}_j$ instead of τ_j and $\eta_j = \bar{\tau}_j.E_j$ in Eq. (14), the viscous parameter of two Maxwell elements are presented in table 3. In all simulations, the Poisson coefficients, necessary for 3D formulation, is arbitrarily selected as: $\nu_1 = \nu_2 = 0.45$.

First Maxwell element	Second Maxwell element
$E_1 = 2.25$ MPa	$E_2 = 0.88$ MPa
$\eta_1 = 28.8$ MPa.s^{-1}	$\eta_2 = 158.$ MPa.s^{-1}

Table 3. The two Maxwell parameters determined analytically with an average value of relaxation times in compression and tension.

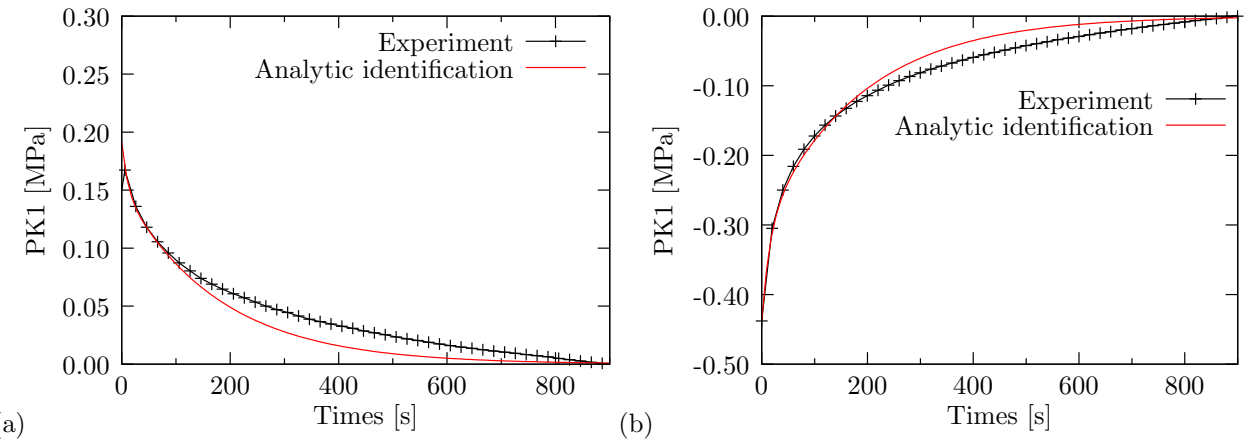

Figure 9. Comparison between experimental data and analytical identification in the displaced stress-time curve. (a) Relaxation-tension test. (b) Relaxation-compression test.

The results of the viscous parameter identification are presented in figures 9(a) and 9(b), in relaxation tests in tension and compression, respectively. As in figure 8(b), a displacement in both time and stress is applied in these figures.

As for hyperelastic and hysteretic parameter identification (section 4.1), using only relaxation test in compression, the obtained analytical viscous parameters are presented in table 4. Comparison with the parameters of table 3 shows that only the first Young's modulus E_1 and the second viscous parameters η_2 are different. However, similar values

are obtained for other parameters, thus showing how little influence loading has in tension or in compression on the viscous response of this material.

First Maxwell element	Second Maxwell element
$E_1 = 1.55$ MPa	$E_2 = 0.75$ MPa
$\eta_1 = 23.85$ MPa.s^{-1}	$\eta_2 = 139.$ MPa.s^{-1}

Table 4. Both Maxwell parameters determined analytically with relaxation time in compression only.

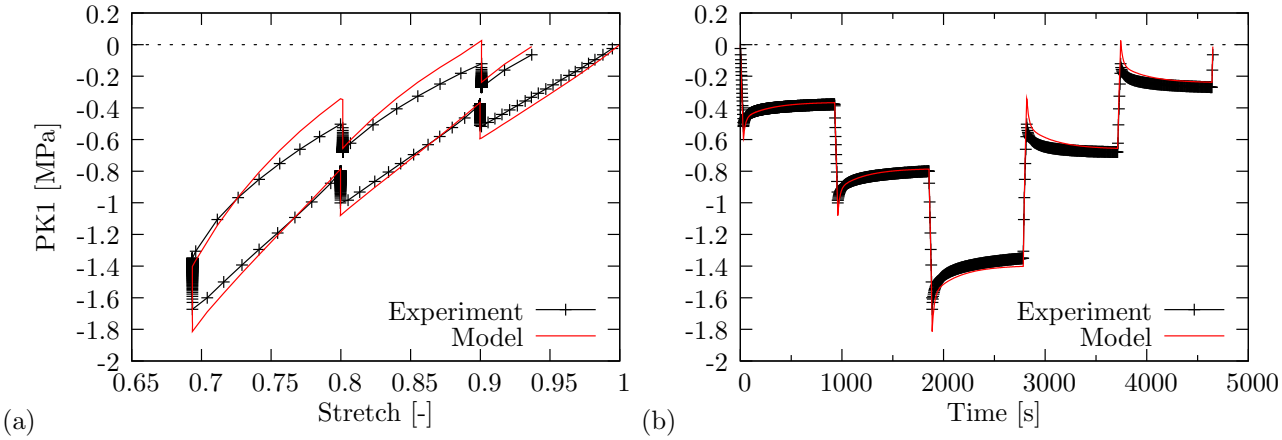

Figure 10. Comparison between experimental and model prediction for the cyclic compression test interrupted by relaxation steps. (a) Stress-stretch response. (b) Stress-time response.

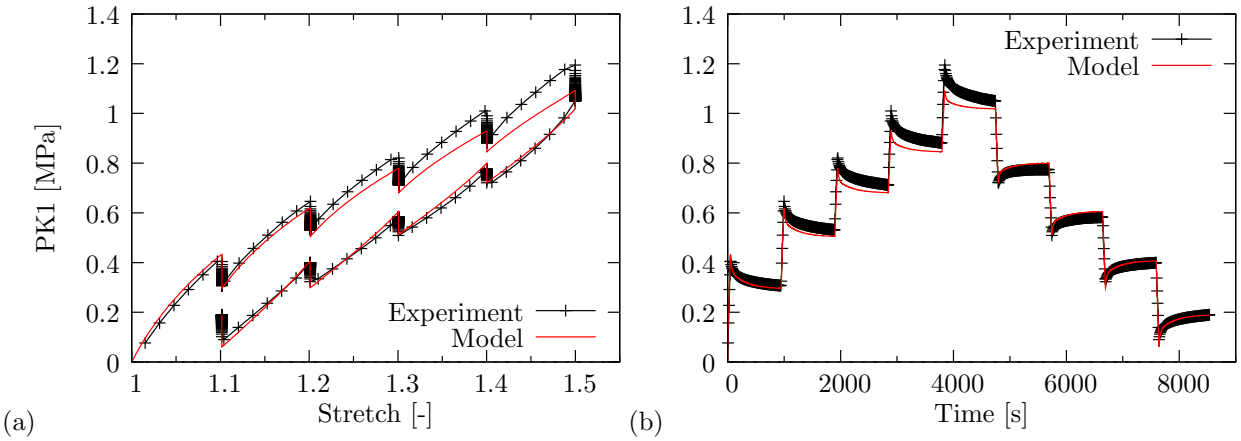

Figure 11. Comparison between experimental and model prediction for the cyclic tension test interrupted by relaxation steps. (a) Stress-stretch response. (b) Stress-time response.

Finally, using the hyperelastic and hysteretic parameters of table 1 and the viscous parameters of table 3, comparisons between experimental and model predictions for the

cyclic compression and tension tests interrupted by relaxation steps, are presented in figures 10 and 11. A better description of these experimental tests is obtained with the procedure herein adopted than with the previous identification using a global inverse numerical method [20]. This procedure is also easier and faster to carry out. Moreover, it discerns all the specific physical phenomena that occur during the mechanical loading of the rubber material.

5. Validation

To verify the pertinence of the HVH model under various loading conditions, based on the parameters herein identified, simulations of experimental tests reported in [20] are performed.

5.1. Complex loadings

The numerical simulations of the complex loading test are carried out in *HEREZH++* program. Experimental boundary conditions are reproduced in a single hexahedral element by imposing experimental loading.

Firstly, the numerical results of relaxation in compression and tension are compared with experimental data in figures 12(a) and 12(b), respectively.

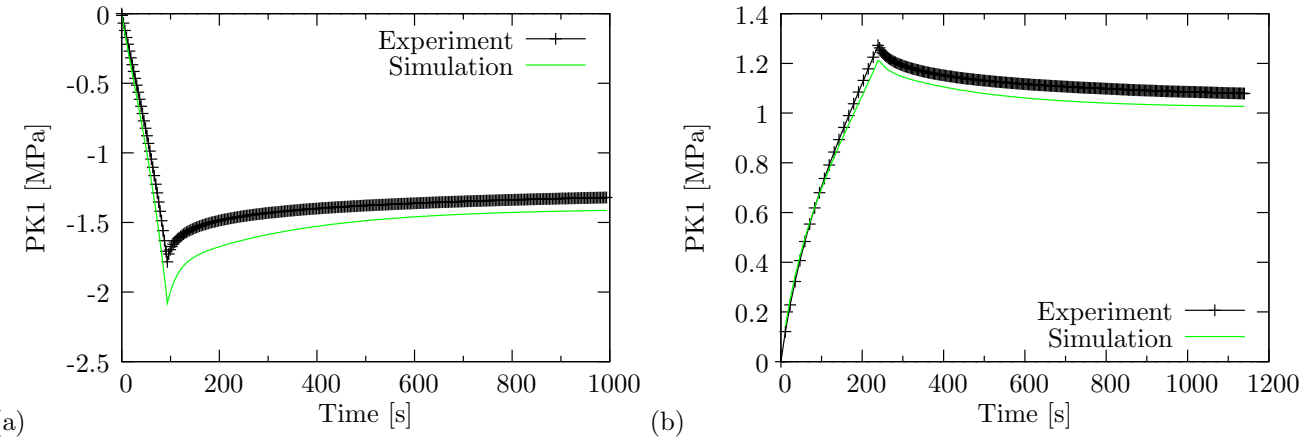

Figure 12. Comparison between experimental and numerical prediction in relaxation test (a) In compression. (b) In tension.

The single cycle of loading-unloading in compression and tension tests and the successive cyclic compression and tension tests are also numerically simulated. Comparisons with experiments are shown in figures 13(a) to 13(b), respectively. Rather good correlation can be observed with some discrepancy in the unloading step for the compression test. Finally, figures 14(a) to 14(b) show that the HVH model gives a reasonable prediction of Mullins' effect, although this is not its initial purpose. This effect is taken into account without introducing any damage parameter.

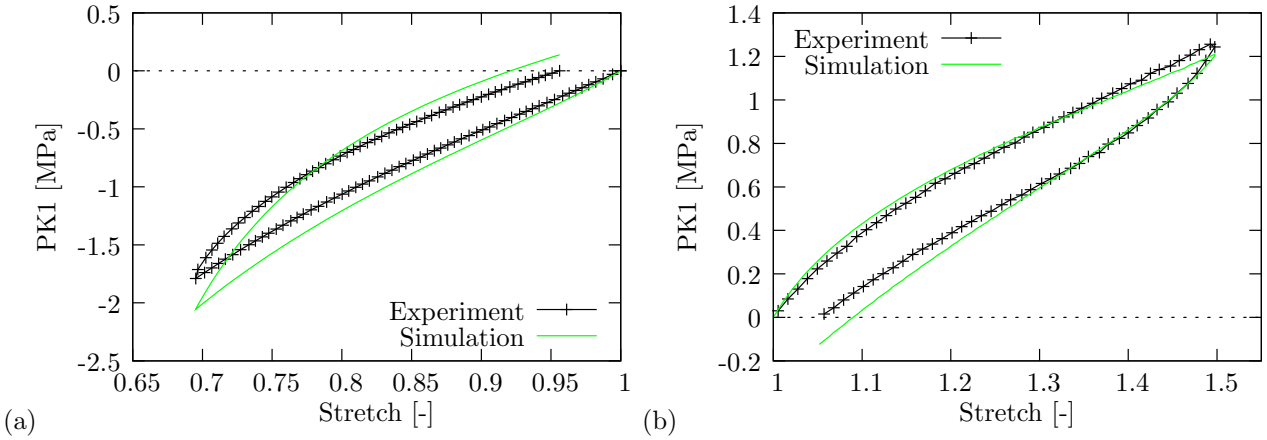

Figure 13. Comparison between experimental and numerical prediction in single cyclic test. (a) In compression. (b) In tension.

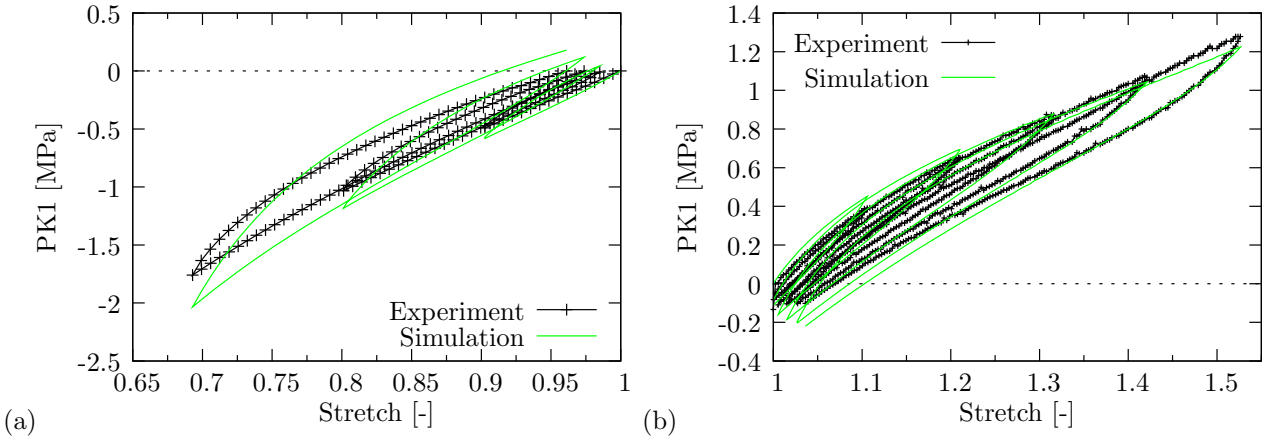

Figure 14. Comparison between experimental and numerical prediction in successive cyclic test. (a) In compression. (b) In tension.

5.2. Industrial o-ring seal under relaxation test

To illustrate the response of the HVH model in the case of an industrial application, an experimental device has been developed to apply a relaxation test on an o-ring seal of Viton rubber. This seal is used to prevent leaking in an oil filter. The square cross-section o-ring is put in a groove and squeezed by a piston of a universal testing machine Instron 4505. Experimental and numerical studies are based on the configuration shown in figure 15 where a cross-sectional view of the model is shown.

During the first step of this test, the piston squeezes the outside diameter of the seal with a strain rate similar to that of previous experimental tests to reproduce the as-installed configuration. Then, a relaxation loading is imposed during 900s and the evolution of the stress is recorded as a function of time. Experimental measurements of the force under the piston have been conducted and repeated three times to verify the reproducibility of the results.

Numerical simulations of this test have been carried out with the FE code

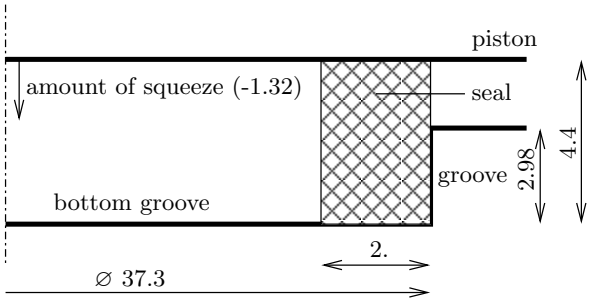

Figure 15. Geometry of the relaxation test on a seal (in mm).

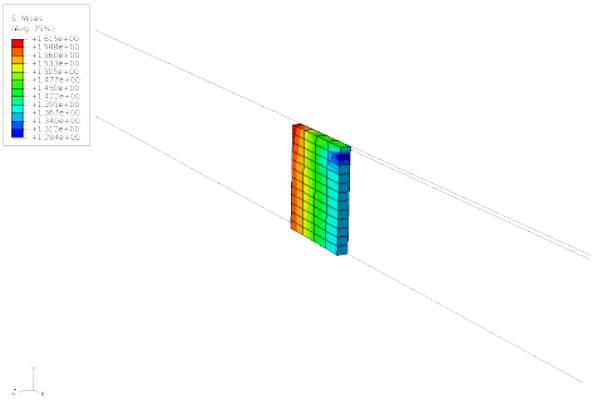

Figure 16. Deformed mesh at the end of relaxation step

ABAQUS, combined with in-house code, *HEREZH++*, according to the software interface presented in [62]. The *HEREZH++* code computes the mechanical behaviour of material in each Gauss point of elements and the software interface ensures communication between *ABAQUS* and *HEREZH++* via the user-defined mechanical material behaviour (Umat). A 3D numerical analysis, with 48 linear eight-node elements, modelling a sector of one degree is achieved with symmetric boundary conditions (figure 16). The piston (top surface) and the groove are considered to be infinitely rigid. Friction between these surfaces and the seal is assumed to be negligible because an oil lubricant is used in actual conditions.

Comparison between numerical results and experimental data is shown in figure 17 in terms of stress as a function of time. Numerical simulations are performed with two kinds of material parameters: firstly, with the parameters obtained from compression and tensile tests (tables 1 and 3) and then with the parameters obtained from compression tests (tables 2 and 4). Good correlation can be observed between numerical predictions and the experiments. This correlation is better when considering material parameters extracted from only compression tests which suggests that compression loading is a predominent state of the simulated o-ring seal.

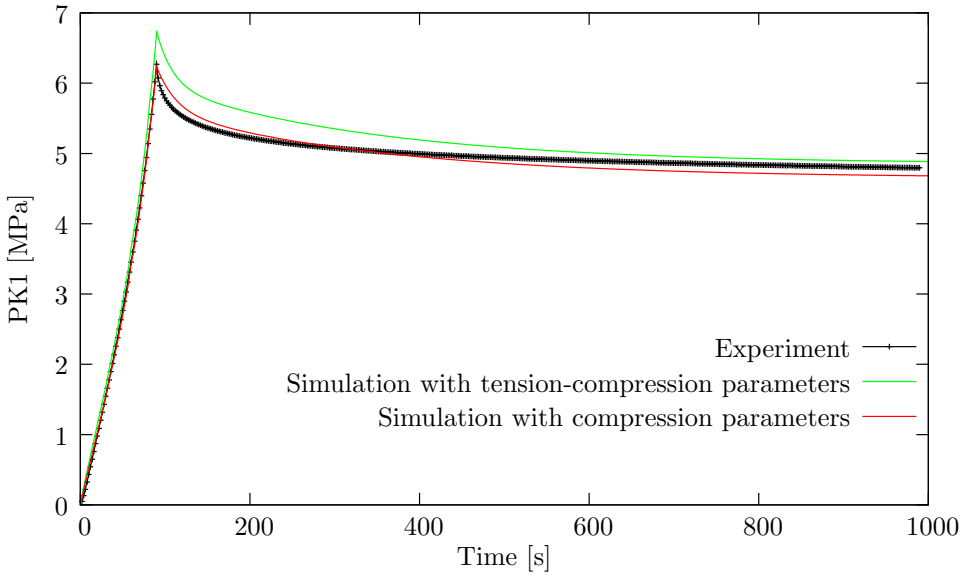

Figure 17. Comparison between experimental data and numerical simulation of an o-ring seal under relaxation test.

6. Conclusion

The determination of behaviour law material parameters is far from being trivial. In this paper, a new identification method is proposed to determine material parameters of an original phenomenological model, named Hyperelasto-Visco-Hysteresis. This model should be able to take several effects into account, which is typical in the case of rubber materials, like strong nonlinearities, hysteresis effects and strain rate-dependent responses. Using the multi-step relaxation tests in tension and compression, the hyperelastic and hysteretic stress contributions of this model are directly estimated. With the simple relaxation tests, the viscous parameters of all Maxwell elements, corresponding to the viscosity stress response, are analytically identified. The main advantage of this method is that, using only a single test, the different responses such as the hyperelasticity, hysteresis and viscosity are discriminated. Accordingly, material parameter identification is substantially easier. Moreover, with this identification procedure can be applied to other polymer materials, if the hyperelastic stress contribution is adequately chosen. With the identified material parameters of the studied fluoro-elastomer, the simulation of tension and compression cyclic tests correspond well with experimental results. Finally, the simulation of a seal under relaxation shows the suitability of the presented constitutive model for practical applications.

References

[1] L. Mullins. Softening of rubber by deformations. *Rubber chemistry and technology*, 42:339–362, 1969.

[2] A. N. Gent. Relaxation processes in vulcanized rubber. I. Relation among stress relaxation, creep, recovery, and hysteresis. *Journal of Applied Polymer Science*, 6(22):433–441, 1962.

[3] L. R. G. Treloar. Stress-strain data for vulcanised rubber under various types of deformation. *Trans. Faraday. SoC.* , 40:59–70, 1944.

[4] J. S. Bergström and M. C. Boyce. Large strain time-dependent behavior of filled elastomers. *Mechanics of Materials*, 32:627–644, 2000.

[5] E. M. Arruda and M. C. Boyce. A three-dimensional constitutive model for the large stretch behavior of rubber elastic materials. *Journal of the Mechanics and Physics of Solids*, 41(2):389–412, 1993.

[6] C. Miehe, S. Göktepe, and F. Lulei. A micro-macro approach to rubber-like materials-Part I: the non-affine micro-sphere model of rubber elasticity. *Journal of the Mechanics and Physics of Solids*, 52(11):2617–2660, 2004.

[7] M. Mooney. A theory of large elastic deformation. *Journal of Applied Physics*, 11:582–592, 1940.

[8] R. S. Rivlin. *Phil. Trans. R. SoC. Lond.*, 240:509–525, 1949.

[9] R. W. Ogden. Large deformation isotropic elasticity- on the correlation of theory and experiment for incompressible rubber like solids. *ProC. Roy. SoC. Lond.*, 326:565–584, 1972.

[10] B. Meissner and L. Matejka. Constitutive equation describing the biaxial stress???strain behavior of poly(dimethylsiloxane) networks reinforced with silica generated in situ. *European Polymer Journal*, 44(7):1940–1948, 2008.

[11] H. Bechir, L. Chevalier, and M. Idjeri. A three-dimensional network model for rubber elasticity: The effect of local entanglements constraints. *International Journal of Engineering Science*, 48(3):253–404, 2010.

[12] M. M. Attard and G. V. Hunt. Hyperelastic constitutive modeling under finite strain. *International Journal of Solids and Structures*, 41:5327–5350, 2004.

[13] L. R. G. Treloar. *The physics of Rubber elasticity*. Clarendon Press, Oxford, 1975.

[14] R. W. Ogden. *Non-linear Elastic Deformations*. Ellis Horwood, Chichester, 1984.

[15] M. C. Boyce and E. M. Arruda. Constitutive models of rubber elasticity. *Rubber Chemistry and Technology*, 73:504–523, 2000.

[16] A. F. M. S. Amin, A. Lion, S. Seikita, and Y. Okui. Nonlinear dependence of viscosity in modeling the rate-dependent response of natural and high damping rubbers in compression and shear: Experimental identification and numerical verification. *International Journal of Plasticity*, 22:1610–1657, 2006.

[17] G. Marckmann and E. Verron. Comparison of hyperelastic models for rubberlike materials. *Rubber Chemistry and Technology*, 79(5):835–858, 2006.

[18] S. Cantournet, R. Desmorat, and J. Besson. Mullins effect and cyclic stress softening of filled elastomers by internal sliding and friction thermodynamics model. *International Journal of Solids and Structures*, 46(11-12):2255–2264, 2009.

[19] J. Lemaitre. *Handbook of Materials Behavior Models*, volume 1. Elsevier, 2001.

[20] A. Vandenbroucke, H. Laurent, N. Aït Hocine, and G. Rio. A Hyperelasto-Visco-Hysteresis model for an elastomeric behaviour: experimental and numerical investigations. *Computational Materials Science*, 48(3):495–503, May 2010.

[21] G. Rio. *Herezh++*. certification IDDN-FR-010-0106078-000-R-P-2006-035-20600, http://web.univ-ubs.fr/lg2m/~rio.

[22] P. Pegon, P. Guélin, D. Favier, B. Wack, and W. Nowacki. Constitutive scheme of discrete memory form for granular materials. *Archives of Mechanics*, 43(1):3–27, 1991.

[23] D. Favier, P. Guélin, and R. Cammarano. Application of a phenomenological elastohysteretic theory to the modeling of magnetization. In *Seventh International Symposium on Magnetic Anisotropy and Coercivity in Rare-Earth Transition Metal Alloys*, pages 137–150, Canberra, Australia, 1992.

[24] P. Y. Manach and N. Couty. Elastohysteresis constitutive law in convected coordinate frames: application to finite deformation shear test. *Computational Mechanics*, 28:17–25, 2002.

[25] G. Rio, D. Favier, and Y. Liu. Elastohysteresis: an accurate phenomenological model for pseudoelasticity and ferroelasticity 3d simulation of shape memory alloys under complex loadings. In *International Conference on Shape Memory and Superelastic Technologies (SMST)*, Stresa, Italy, 2008.

[26] G. Blès, W. K. Nowacki, and A. Tourabi. Experimental study of the cyclic visco-elasto-plastic behaviour of a polyamide fibre strap. *International Journal of Solids and Structures*, 46(13):2693–2705, 2009.

[27] M. Zrida, H. Laurent, G. Rio, S. Pimbert, V. Grolleau, N. Masmoudi, and C. Bradai. Experimental and numerical study of polypropylene behavior using an hyper-visco-hysteresis constitutive law. *Computational Materials Science*, 45(2):516–527, 2009.

[28] M. Brieu, J. Diani, and N. Bhatnagar. A new biaxial tension test fixture for uniaxial testing machine - A validation for hyperelastic behavior of rubber-like materials. *Journal of Testing and Evaluation*, 35, 2007.

[29] G. Chagnon, E. Verron, G. Marckmann, and L. Gornet. Development of new constitutive equations for the mullins effect in the rubber using the network alteration theory. *International Journal of Solids and Structures*, 43:6817–6831, 2006.

[30] SiDoLo. *P. Pilvin*. User's Manual in French, http://web. univ-ubs.fr/lg2m/˜pilvin/sidolo.pdf.

[31] A. Andrade-Campos, S. Thuillier, P. Pilvin, and F. Teixeira-Dias. On the determination of material parameters for internal variable thermoelastic-viscoplastic constitutive models. *International Journal of Plasticity*, 23(8):1349–1379, 2007.

[32] A. Lion. On the large deformation behaviour of reinforced rubber at different temperatures. *Journal of the Mechanics and Physics of Solids*, 45:1805–1834, 1997.

[33] J. S. Bergström and M. C. Boyce. Constitutive modeling of the large strain time-dependent behavior of elastomer. *Journal of Mechanical and Physics of Solids*, 5:931–954, 1998.

[34] A. Lion. A constitutive model for carbon black filled rubber: Experimental investigation and mathematical representation. *Continuum Mechanics and thermodynamics*, 8:153–169, 1996.

[35] A. F. M. S. Amin, M .S. Alam, and Y. Okui. An improved hyperelasticity relation in modelling viscoelasticity response of natural and high damping rubbers in compression: experiments, parameters identification and numerical verification. *Mechanics of Materials*, 34:75–95, 2002.

[36] J. Diani, M. Brieu, and J. M. Vacherand. A damage directional constitutive model for Mullins effect with permanent set and induced anisotropy. *European Journal of Mechanics - A/Solids*, 25(3):483–496, 2006.

[37] A. R. Bhuiyan, Y. Okui, H. Mitamura, and T. Imai. A rheology model of high damping rubber bearings for seismic analysis: Identification of nonlinear viscosity. *International Journal of Solids and Structures*, 46(7-8):1778–1792, 2009.

[38] C. Miehe and J. Keck. Superimposed finite elastic-viscoelastic-plastoelastic stress response with damage in filled rubbery polymers. Experiments, modelling and algorithmic implementation. *Journal of the Mechanics and Physics of Solids*, 48(2):323–365, 2000.

[39] E. M. Dannenberg. The effects of surface chemical interactions on the properties of filler-reinforced rubber. *Rubber Chem. Technol.*, 48:410–442, 1975.

[40] H. G Kilian, M. Strauss, and W. Hamm. Universal properties in filler loaded rubbers. *Rubber Chem. Technol.*, pages 1–16, 1994.

[41] F. Buehe. Molecular basis for the mullins effect. *Journal of Applied Polymer Science*, 4(10):107–114, 1960.

[42] S. Govindjee and J. C. Simo. Mullins effect and the strain amplitude dependence of the storage modulus. *International Journal of Solids and Structures*, 29(14-15):1737 – 1751, 1992.

[43] A. S. Khan and O. Lopez-Pamies. Time and temperature dependent response and relaxation of a soft polymer. *International Journal of Plasticity*, 18:1359–1372, 2002.

[44] R. C. Lin and U. Schomburg. A finite elastic-viscoelastic-elastoplastic material law with damage: theoretical and numerical aspects. *Computer Methods in Applied Mechanics and Engineering*, 192(13-14):1591–1627, 2003.

[45] D. Besdo and J. Ihlemann. A phenomenological constitutive model for rubberlike materials and its numerical applications. *International Journal of Plasticity*, 19:1019–1036, 2003.

[46] K. Hasanpour and S. Ziaei-Rad. Finite element simulation of polymer behaviour using a three-dimensional, finite deformation constitutive model. *Computers & Structures*, 86(15-16):1643–1655, 2008.

[47] L. A. Gracia, E. Liarte, J. L. Pelegay, and B. Calvo. Finite element simulation of the hysteretic behaviour of an industrial rubber. Application to design of rubber components. *Finite Elements in Analysis and Design*, 46(4):357–368, 2010.

[48] G. A. Holzapfel. *Non linear solid mechanics*. Johns Wiley & Sons, Chichester, England, 2000.

[49] Y. Basar and D. Weichert. *Nonlinear Continuum Mechanics of Solids*. Springer Verlag Berlin Heidelberg, New-York, 2000.

[50] G. Blès. *Bases thermomécaniques de la modélisation du comportement des matériaux tissés et des polymères solides*. PhD thesis, Université Joseph Fourier - Grenoble I, 2002.

[51] P. Guélin. Remarques sur l'hystérésis mécanique. *Journal de Mécanique Théorique et Appliquée*, 19(2):217–245, 1980.

[52] D. Favier and P. Guélin. A discrete memory constitutive scheme for mild steel type material theory and experiment. *Archives of Mechanics*, 37(3):201–219, 1985.

[53] D. Favier, P. Guélin, and P. Pegon. Thermomechanics of hysteresis effects in shape memory alloys. *Materials Science Forum*, 56-58:559–564, 1990.

[54] R. S Rivlin. Large elastic deformations. *Rheology-Theory and applications*, 1:351–285, 1956.

[55] L. J Hart-Smith. Elasticity parameter for finite deformation of rubber-like materials. *Zeitschrift fur Angewandte Mathematik und Physik*, 17:608, 1966.

[56] C. Moreau. *Etude expérimentale et Numérique de l'Hyperélasticité avec prise en compte de l'incompressibilité*. Thèse de doctorat, Université de Bretagne Sud, 2000.

[57] I. M. Ward and J. Sweeney. *An introduction to the mechanical properties of solid polymers*. John Wiley and Sons, 2004.

[58] M. Kaliske and H. Rothert. Formulation and implementation of three-dimensional viscoelasticity at small and finite strains. *Computational Mechanics*, 19(3):228–239, 1997.

[59] C. Joubert, A. Michel, L. Choplin, and P. Cassagnau. Influence of the crosslink network structure on stress-relaxation behavior: Viscoelastic modeling of the compression set experiment. *Journal of Polymer Science Part B: Polymer Physics*, 41(15):1779–1790, 2003.

[60] J. Diani, M. Brieu, and P. Gilormini. Observation and modeling of the anisotropic visco-hyperelastic behavior of a rubberlike material. *International Journal of Solids and Structures*, 43(10):3044–3056, 2006.

[61] S. Reese and S. Govindjee. A theory of finite viscoelasticity and numerical aspects. *International Journal of Solids and Structures*, 35:3455–3482, 1998.

[62] G. Rio, H. Laurent, and G. Blès. Asynchronous interface between a finite element commercial software ABAQUS and an academic research code HEREZH++. *Advances in Engineering Software*, 39(12):1010–1022, 2008.